Selective Area Heteroepitaxy of p-i-n Junction GaP Nanopillar Arrays on Si (111) by MOCVD

Wonsik Choi, Hsien-Chih Huang, *Graduate Student Member, IEEE*, Shizhao Fan, Parsian K. Mohseni, Minjoo Larry Lee, *Member, IEEE*, and Xiuling Li, *Fellow, IEEE*

***Abstract*— Gallium phosphide (GaP) is an important optical material due to its visible wavelength band gap and high refractive index. However, the bandgap of the thermodynamically stable zinc blende GaP is indirect, but wurtzite (WZ) structure GaP is direct bandgap. In this work, we demonstrate high-quality and dense GaP vertical nanopillar (NP) array directly on Si (111) substrates through selective area epitaxy (SAE) by MOCVD for the first time, through systemic studies of the effect of TMGa flow rate, growth temperature, and V/III ratio. Uniform GaP NPs are grown over a patterned 400 μm × 400 μm area with 97.5% yield. Arrays of GaP vertical p-i-n NP diodes are demonstrated with a ideality factor and rectification ratio of 3.7 and 103, respectively. With the high yield of hexagonal structure and electrically proven device quality of GaP NPs through this growth method, this work represents a significant step in achieving GaP NP based optoelectronic devices, such as micro-LEDs emitting in the green wavelength range.**

***Index Terms*— Gallium phosphide, selective area epitaxy, nanopillar, nanowire, MOCVD.**

I. Introduction

THE vapor-liquid-solid (VLS) mechanism has been used to grow nanowires (NWs) for decades due to its precise control of high crystal quality growth for many III-V semiconductor NWs [1], [2]. Nonetheless, it is not always desirable for VLS grown NWs to be monolithically integrated in conventional silicon (Si) based technology, because the metal particle used for VLS growth could be incorporated as an unintentional impurity dopant in Si and induce deep levels that degrade device properties by trapping electrons and holes [3]. An alternative technique to grow NWs without the usage of metal nanoparticle catalysts is the selective-area-epitaxy (SAE) method [4]–[6]. Fig. 1a illustrates the typical growth steps of SAE. In this NW growth mechanism, the location and size of NW are defined by lithographically patterned and wet/dry etched openings of the amorphous thin film mask, such as silicon dioxide (SiO_2) or silicon nitride (SiN_x), which are deposited on top of a single crystal substrate [7]. When gaseous sources are introduced to the mask patterned substrate under specific conditions (growth temperature, pressure, molar flow rate of the precursors, V/III ratio, etc.), single crystal NWs can be selectively grown only in the exposed regions. It is known that III-V NWs are preferentially grown in <111>A or <111>B directions, and vertically aligned array of III-V NWs can be formed on top of the (111)A or (111)B III-V substrates [8]. In addition, heteroepitaxial growth of III-V SAE NWs on top of Si (111) substrates enables direct integration of III-V-based high-mobility and direct bandgap optoelectronic devices on the conventional Si platform [9], [10].

Among the III-V compound semiconductors, gallium phosphide (GaP) is one of the promising optical materials due to its unique bandgap that falls in the visible range at 2.26 eV, and a high refractive index of 3.37 [11], [12]. In addition, its thermo-optical coefficient and mechanical properties in comparison to materials with a similar transmission range, enables GaP to be applied to flexible optical devices that can perform in harsh weather conditions [12]. Recently, the growth of GaP NWs on several substrates using a variety of NW growth methods have been reported [13]–[20]. GaP NWs most frequently studied are the homoepitaxially growing NWs on top of GaP (111)B substrates via the VLS mechanism using gold catalysts [14], [17], [18], [21], [22] GaP NWs have also been heteroepitaxially synthesized on top of Si (111) [13], [16], [20] and Si (100) substrates [18] using the VLS method. Moreover, the GaP SAE NW shell growth on Indium Phosphide (InP) core NWs grown on InP (111)B substrate has also been reported [15]. However, SAE growth of GaP NWs directly on Si (111) substrates are not well reported yet.

In this work, we demonstrate dense, ordered, and uniform GaP NW array grown on Si (111) substrates by MOCVD via the SAE mechanism for the first time. Note that we use nanowire (NW) and nanopillar (NP) interchangeably hereafter due to different definitions in the community, but all NW or NP dimensions are described. The effects of TMGa flow rate, growth temperature, and III/V ratio are systematically studied and a 97.5% yield of GaP NPs is achieved. In addition, Si and Zn doping are introduced to form GaP p-n and p-i-n vertical NPs. Finally, GaP NP vertical diodes are fabricated and electrically characterized.

Manuscript received 6 December 2021; revised 3 February 2022; accepted 8 February 2022. Date of publication 16 February 2022; date of current version 28 July 2022. This work was supported in part by the National Science Foundation (NSF) through the Division of Materials Research under Grant 1508140 and Electrical, Communications and Cyber Systems (ECCS) under Grant 18-09946. *(Corresponding author: Xiuling Li.)*

Wonsik Choi, Hsien-Chih Huang, and Minjoo Larry Lee are with the Micro and Nanotechnology Laboratory, Department of Electrical and Computer Engineering, University of Illinois at Urbana-Champaign, Urbana, IL 61801 USA.

Shizhao Fan was with the Micro and Nanotechnology Laboratory, Department of Electrical and Computer Engineering, University of Illinois at Urbana-Champaign, Urbana, IL 61801 USA. He is now with the Suzhou Institute of Nano-Tech and Nano-Bionics (SINANO), Suzhou 215123, China.

Parsian K. Mohseni was with the Micro and Nanotechnology Laboratory, Department of Electrical and Computer Engineering, University of Illinois at Urbana-Champaign, Urbana, IL 61801 USA. He is now with the Rochester Institute of Technology (RIT), Rochester, NY 14623 USA.

Xiuling Li was with the Department of Electrical and Computer Engineering, University of Illinois at Urbana-Champaign, Urbana, IL 61801 USA. She is now with the Microelectronics Research Center, Department of Electrical and Computer Engineering, The University of Texas at Austin, Austin, TX 78758 USA (e-mail: xiuling.li@utexas.edu).

This article has supplementary material provided by the authors and color versions of one or more figures available at https://doi.org/10.1109/JQE.2022.3151971.

Digital Object Identifier 10.1109/JQE.2022.3151971

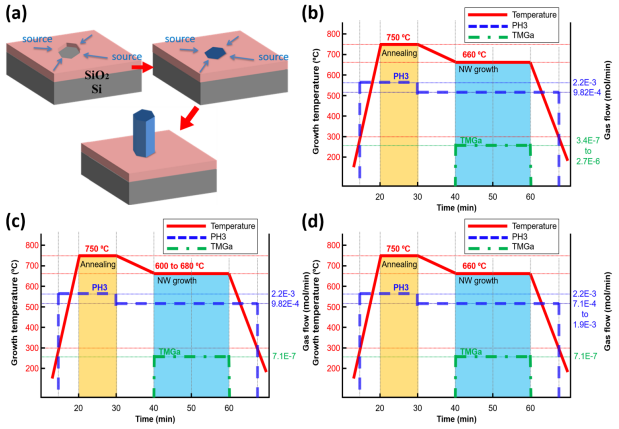

Fig. 1. (a) Schematic of the SAE growth of NP on a SiO_2 patterned Si substrate. The gaseous sources are introduced to the lithographically defined SiO_2/Si substrate and the vertical NP is grown on the specific opened region. (b-d) Schematic illustration of the sequence of gas flow and growth temperature during GaP NP growth with varying (b) TMGa flow rate, (c) growth temperature and (d) PH_3 flow rate.

II. Experimental Methods

GaP NPs were grown on SiO_2 patterned Si (111) substrates, provided by Imec. Specifically, 20 nm of SiO_2 were deposited onto the Si (111) surface and 10 × 10 arrays of circles of 100 nm diameter and 300 nm pitch were patterned by a proprietary method. Before loading, the substrate was etched with 1:50 HF:H_2O solution to ensure the removal of the native oxide in the openings for growth. Note that patterning methods do not significantly impact the growth quality, but removing the native oxide completely is critical. The patterned substrates were then loaded into a Aixtron Close Coupled Showerhead MOCVD chamber set at 100 mbar of growth pressure. Trimethyl gallium (TMGa) and phosphine (PH_3) were used as group-III and group-V precursors, respectively. Since GaP NPs are preferentially grown along the <111>B direction, [16] the substrates of NPs require the selection of the (111)B-oriented surface (group-V terminated surface) to achieve vertically aligned NPs; while on the (111)A-oriented surface (group-III terminated surface), III-V NPs grow along three tilted direction (19.5° from the surface) [1], [8], [10]. However, unlike III-V materials, Si does not have surface polarity; therefore, the surface of Si has to be modulated as (111)B-oriented in order to control the direction of NPs [8], [10]. To achieve group-V terminated surface on the Si(111) substrate, 50 sccm (2.2×10^{-3} mol/min) of PH_3 was introduced during the ramping up/native oxide desorption step (750 °C for 10 min). After the desorption/annealing step, the gas flow rate of PH_3 was adjusted to the specific NP growth condition and the chamber temperature was reduced to the NP growth temperature. TMGa source was only introduced into the chamber when the system reached the growth temperature necessary to grow GaP NPs. Following the NP growth, TMGa source was immediately cut off while PH_3 flow was maintained to prevent the evaporation of phosphorous in the grown NPs until the chamber temperature cooled down to 300 °C.

III. Results and Discussion

A. Effect of TMGa Flow Rate

To achieve high-quality MOCVD-grown GaP NPs on Si substrates, the effect of TMGa gas flow rate on the yield and morphologies of GaP NPs was first studied. The flow rate of TMGa was varied from 3.4×10^{-7} to 2.7×10^{-6} mol/min, while the PH_3 gas flow was fixed at 9.82×10^{-4} mol/min (Fig. 1b), corresponding to a V/III ratio from 364 to 2890. The growth temperature was ramped down and fixed at 660°C after annealing under PH3 at 750°C for 10 mins. As shown by the top-view and 30° tilted SEM images in Fig. 2, the TMGa flow rate modulation resulted in GaP nanostructures with four different types of topography. The first type of structure (indicated as "A" in Fig. 2) is a vertically grown nanopillar with a perfect symmetric hexagonal top flat surface surrounded by six {1-10} sidewalls. The second one is a nano-pillar structure with a pinched-off top surface with unequal asymmetric sidewalls ("B" in Fig. 2). The third one is a bulky nano-pillar with random shapes ("C" in Fig. 2). The last one (labeled as "D" in Fig. 2) is a hexagonally bounded nanostructures with three {-1-10} top facets and six short vertical {1-10} side facets. Because the morphology and uniformity of NPs are critical to the NP based device properties, the yield of NPs was calculated by counting the number of vertically grown perfect hexagonal surfaced NP (Type A) for this study. A set of representative SEM images of NPs grown under different TMGa flow rates are shown in Fig. 3a–d, and the average NP height and Type A nanopillar yield as a function of TMGa flow rate are plotted in Fig. 3e. When the TMGa flow rate was high (2.7×10^{-6} mol/min), only Type C and D nanostructures were observed (Fig. 3a). Vertical NPs of Type A and B started to appear (Fig. 3b), when the TMGa flow rate decreased to 1.0×10^{-6} mol/min. As the TMGa flow was further reduced to 7.1×10^{-7} mol/min (Fig.3c), the percentage of Type A NP greatly increased to as high as 90%, without showing any Type C and D undesirable nanostructures. After the gas flow of TMGa was reduced (4.8×10^{-7} mol/min), the yield of Type A NP decreased again and void holes without any growths appeared due to the lack of nucleation of materials (Fig. 3d). The height of the hexagonal NP decreased by reducing the TMGa gas flow rate, because the amount of the group III source determines the growth rate of NP under the fixed group-V flow condition. Type D nanostructured NPs have also been reported in GaAs SAE NP growth studies previously, [23]–[27] and was attributed to the different growth rates between the (111)B and (110) planes, which are functions of temperature and V/III ratio [28]. At a higher growth temperature and a low V/III ratio, the growth rate of the (111)B surface is much faster than that of the (110) planes, and the pinched tetrahedral with three {-1-10} top facets and six {1-10} short side facets of type D structure is favored [23]. However, when the V/III ratio is increased, the growth rate of

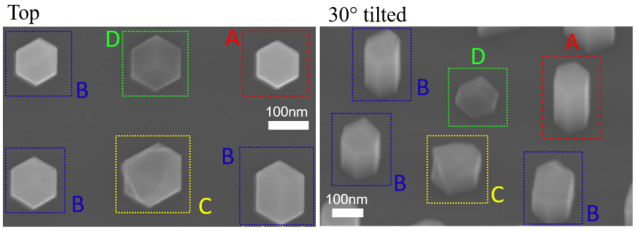

Fig. 2. SEM images of four different types of nanostructures that appeared in the GaP NP growth study. Top view is shown in the left panel and the corresponding 30° tilted image is shown in right panel.

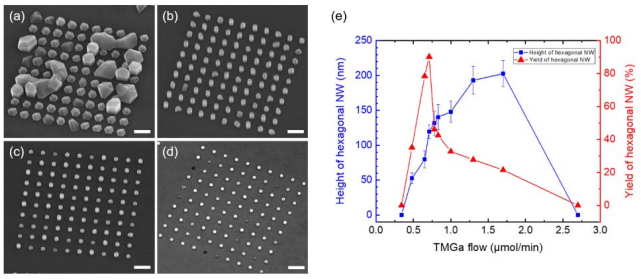

Fig. 3. 30° tilted SEM images of GaP NPs under TMGa flow rate of (a) 2.7×10^{-6}, (b) 1.7×10^{-6}, (c) 7.1×10^{-7}, and (d) 4.8×10^{-7} mol/min. Scale bars represent 400 nm. (e) Plot of average height (left axis) and yield (right axis) of hexagonal NPs (Type A) as a function of TMGa flow rate in μmol/min.

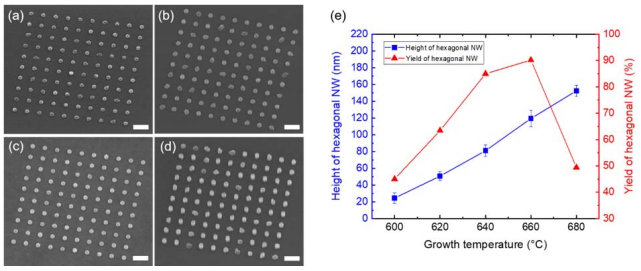

Fig. 4. 30° tilted SEM images of GaP NPs under the growth temperature of (a) 600, (b) 620, (c) 660, and (d) 680 °C. Scale bars: 400 nm. (e) Plot of the average height and yield of hexagonal NPs as a function of the growth temperature.

{-1-10} facets increases so that the vertical NP occupied by six {1-10} side facets with a flat hexagonal (111)B surface NP (Type A) can be grown [23].

B. Effect of NP Growth Temperature

We then studied the dependence of the growth yield and morphologies of GaP NPs on the growth temperature under a fixed gas flow rate of TMGa (7.1×10^{-7} mol/min) and PH_3 (9.82×10^{-4} mol/min) by varying growth temperatures ranging from 600 °C to 680 °C (Fig. 1c). Fig. 4a–d shows the 30° tilted SEM images of NPs grown at 600, 620, 660, and 680 °C, respectively. The average height and yield of the hexagonal NPs as a function of growth temperature (600–680 °C) are plotted in Fig. 4e. The average height of NPs steadily increased from 24.3 nm to 152.4 nm when growth temperature increased from 600 to 680 °C because of the increment of adatom diffusion length with increasing temperature [29]. In addition, it was observed that the diameters of NPs grown at lower temperatures are larger than the those at higher temperatures (up to 660 °C). It can be concluded that the increase of the NP height with respect to the growth temperature is consistent with the preferential NP grow laterally rather than axially at lower growth temperatures [30]. In this respect, the yield of NPs increased up to ~90 % as the growth temperature increased to 660 °C, because the lateral overgrowth, which induces different crystal structures, [29] is only prevalent at lower temperatures. However, when the growth temperature was further increased to 680 °C, the yield of type A NP dramatically decreased again because the tetrahedral nanostructure preferentially appears at a higher temperature and under a certain fixed gas source flown condition [23], [24].

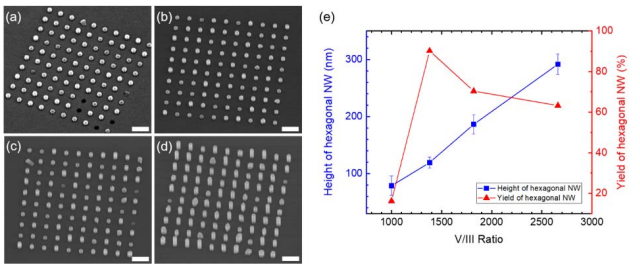

Fig. 5. 30° tilted SEM images of GaP NPs under the four different V/III ratios of (a) 1,000, (b) 1,380, (c) 1,820, and (d) 2,660, with a 400 nm scale bar. (e) Plot of the average height and yield of the GaP NPs as a function of the V/III ratio.

C. Effect of V/III Ratio

The contribution of the V/III ratio of the GaP SAE NP growth was investigated by modulating the flow rate of the group-V source from 7.14×10^{-4} to 1.9×10^{-3} mol/min while fixing the group-III flow rate at 7.1×10^{-7} mol/min to achieve 1,000 to 2,660 of the V/III ratios and the growth temperature at 660 °C (Fig. 1d). The SEM images shown in Fig. 5a–d are the GaP SAE NPs grown under the V/III ratios of 1,000, 1,380, 1,820, and 2,660, respectively. The average height and yield of the hexagonal NP are shown in Fig. 5e. Under the low PH_3 flow rate (Fig. 5a), void holes without any material growth were observed because the nucleation probability of NP was decreased. Type D nanostructures also appeared under this low V/III ratio condition. When the V/III ratio was increased to 1,380, Type D nanostructure disappeared and the high yield (~90 %) of the hexagonal NP was achieved. However, further increment of the V/III ratio induced radial growth so that the percentage of Type A NP was decreased again [31]. The height of NP increased from 78.7 nm to 291.7 nm when the V/III ratio was increased.

D. XRD Measurements of GaP SAE NPs

Based on the above systemic studies of GaP NP growth on TMGa flow rate, growth temperature, and V/III ratio, it was determined that a high yield of the hexagonal (Type D) GaP NPs can be achieved at 660 °C growth temperature, 7.1×10^{-7} mol/min TMGa flow rate, 9.82×10^{-4} mol/min PH_3 flow rate, and 1380 V/III ratio. It is well known that the III-P materials are in cubic zinc blend (ZB) structure in bulk, whereas the III-nitrides are in hexagonal wurtzite (WZ) structure. However, the crystal structure of the III-V materials can be changed when they are grown in NW *via* the VLS/SAE mechanism so that either a ZB, WZ, or an intermixing of the ZB and WZ structured III-V NWs can be achieved [32]. This modulation of the crystal structure is interesting, especially in GaP material, because the WZ structured GaP has a direct band gap between 2.18 and 2.25 eV, [18], [33] which is desirable for a green-yellow range of LEDs [14] and solar water splitting devices, [17] while the ZB GaP has 2.97 eV of indirect band gap [33]. Recently, the growth of WZ structured III-V NWs have been reported [8], [14], [29], [31], [32], [34]–[41]. The realization of WZ NWs were experimentally verified but the mechanism of selecting a crystal structure while NW is grown are still controversial [41]. However, a common factor that promotes

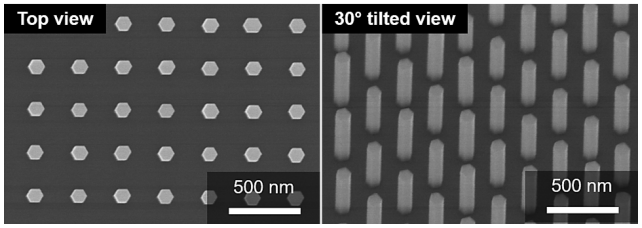

Fig. 6. Top view and 30° tilted view SEM images of the p-n axial junction GaP NP grown on an n-Si (111) substrate.

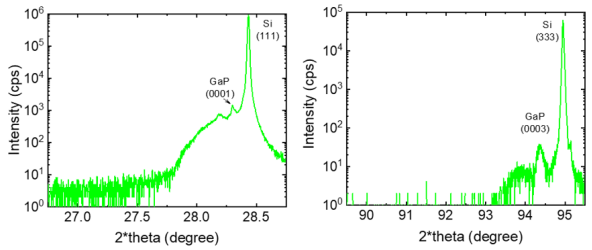

Fig. 7. XRD curves measured from the GaP NPs on Si(111) sample shown in Fig. 6. The peak is aligned based on the Si (333) peak from the substrate.

the realization of WZ structured NW is the suppression of the lateral overgrowth, because the ZB structure has the lowest surface energy at {1-11} side facets of the hexagonal NW [31]. On the other hand, the nucleation on side {1-100} facets of WZ NW is difficult so that the hexagonal WZ NWs tend to grow more vertically with less lateral overgrowth [39]. Consequently, it can be inferred that GaP NWs grown under the optimized growth condition would form a WZ structure. With the purpose of fabricating an array of GaP SAE NPs based photodetector, GaP SAE NPs were successfully grown on a larger area (400 μm $\times$ 400 μm) with denser openings (opening holes of 100 nm in diameter with a 200 nm distance) and a 97.25% yield of the hexagonal NPs uniformly on all the patterns. The SEM images of GaP NPs are shown in Fig. 6 with an average diameter of 103 nm and 3.8 nm standard deviation. To verify the crystal structure of GaP NPs, the NP lattice parameter was determined by XRD, and the results are shown in Fig. 7. The peak was aligned based on the Si (333) peak detected from the substrate. Relatively broad GaP(0003) and GaP(0001) peaks were observed and 6.3016 Å of the c-lattice parameter was obtained, consistent with that of WZ GaP. In addition, room temperature photoluminescence (PL) characterization was conducted on the GaP NPs. As shown in Fig. S1, the PL spectra exhibits a board peak at around 1.96 eV. The peak matches with the predicted inter-band transition, Γ_{9v} to Γ_{8c}, and the results of other reported WZ GaP, [14] suggesting GaP nanopillars grown might be in WZ structure. Note that because of the broad peaks attributed to GaP in both XRD and PL, there is uncertainty in assigning the GaP NP crystal structure to pure WZ or a mixture of ZB and WZ. Further characterization including absorption spectroscopy and transmission electron microscopy (TEM) needs to be carried out to confirm the WZ structure.

E. Arrays of GaP SAE NP Axial pn Junction Diode

To examine the electrical qualities of these NPs, an array of GaP NP diodes were fabricated with on an n-type Si (111) substrate. To achieve an axial p-n junction NP, disilane (Si_2H_6)

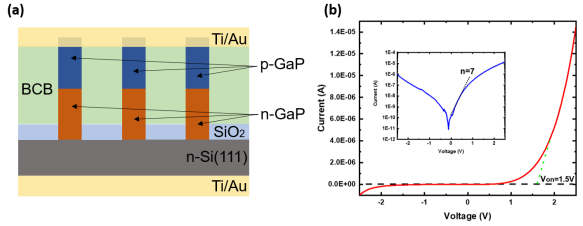

Fig. 8. (a) Schematic of the array of the fabricated p-n junction GaP NP diode. (b) I-V curves of the p-n junction GaP NP diode. The inset shows the semilogarithmic plot of the I-V curve.

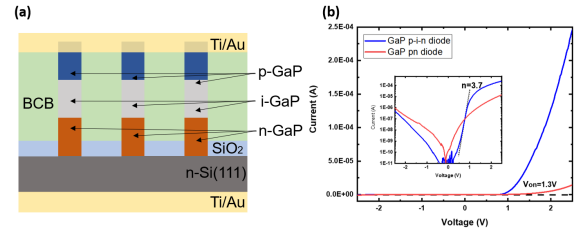

Fig. 9. (a) Schematic of the array of the p-i-n junction GaP NP diode. (b) I-V curves of the p-i-n junction GaP NP diode (solid blue line) and p-n junction GaP NP diode (solid red line). The inset shows the semilogarithmic plot of the I-V curve. The diameter, distance, and height of the NP were 100 nm, 250 nm, and 900 nm, respectively.

and dimethyl zinc (DMZn) were introduced sequentially as n-type and p-type dopant sources, respectively, while TMGa and PH_3 were supplied constantly during the entire NP growth period. The detailed growth condition is listed in the supporting information. The height of each n and p segment of NP was estimated at approximately 260 nm each because the n- and p-type dopants were introduced for the same amount of time. After the SAE growth, planarization process with benzocyclobutene (BCB) was conducted and followed by RIE etching to reveal the NP top for contact. Then, a Ti/Au (10 nm/140 nm) metal contact was deposited on top of the exposed area of the NP, and a layer of Ti/Au (20 nm/100 nm) was deposited on the back of the n-type Si substrate (Fig. S2).

The I-V characteristics of the GaP NP diodes are shown as Fig. 8. A well-defined rectifying I-V characteristic is observed with a turn-on voltage of 1.5 V. The inset of Fig. 8b shows the semilogarithmic plot of the I-V curve. A relatively high estimated ideality factor of 7 was extracted from the slope of the semilogarithmic I-V curve and a relatively low on/off ratio of 10 was detected at $\pm$ 2.5 voltage due to high leakage current in the negative-bias region. The high ideality factor and leakage current could be attributed to the carrier tunneling across the junction in the GaP NP, [42] especially with high doping concentration of the n and p-NPs.

To reduce the leakage current and ideality factor of the highly doped GaP NP, an un-doped intrinsic GaP segment was introduced between the n-type and p-type GaP NPs (Fig. S3). The growth conditions were identical to the GaP p-n NPs, except no doping source was introduced during intrinsic section growth. The length of the n, i, and p segments of the GaP NP is estimated to be 300 nm each based on the growth time. Then, the same diode fabrication process was performed on the NPs to produce GaP p-i-n vertical diodes (Fig. 9a).

Fig. 9b shows the I-V characteristics of p-n and p-i-n GaP NP diodes. Similar to the p-n diode, the p-i-n diode demonstrates a rectifying I-V characteristic with a 1.3 V turn-

on voltage. In contrast, an ideality factor of 3.7 was extracted (inset of Fig. 9b), which is much lower compared to the value of p-n NPs. The on/off ratio of the p-i-n diode was also greater by two orders of magnitude than the pn diode. These improvements suggest the severe carrier tunneling at the narrow depletion region of the GaP p-n NP was reduced by the intrinsic segment of the NP. The large ideality factor (> 2) may be caused by the structural defects, such as stacking faults, within the nanopillars or the surface states induced by RIE damages during the fabrication process of the NP diode. We believe that the ideality factor of a diode is expected to be further reduced by passivating the NP surface with an oxide layer before performing the BCB RIE process.

IV. Conclusion

In conclusion, we have demonstrated high-quality and dense GaP nanopillar array on the Si (111) substrate through SAE MOCVD growth for the first time. Four type GaP nanopillars were observed after the SAE growth and among them, the pure WZ structure GaP nanopillar (type A in the paper) is desired due to its direct bandgap property. Then, the effect of TMGa flow rate, growth temperature and III/V ratio are studied in detail to determine the recipe with best yield. Under high TMGa flow rate, GaP nanopillars with undesired random shapes (type C) and hexagonally bounded nanostructures with three top facets (type D) are mostly grown. In addition, the vertical NP growth rate and the yield are found to increase with the growth temperature due to the increment of adatom diffusion length. Finally, the optimization of III/V ratio is conducted and a 97.5% yield of the hexagonal GaP NPs is achieved with the 660 °C growth temperature, 7.1 × 10-7 mol/min TMGa flow rate, and 1380 V/III ratio. The XRD and PL measurement suggests the GaP nanopillars are in WZ structure. Finally, the Si and Zn doping are introduced during the growth to fabricate GaP p-n and p-i-n vertical NP diodes. A rectifying I-V behavior with 1.3 V turn-on voltage, 3.5 ideality factor and ∼ 103 on/off ratio is observed in the GaP p-i-n diode. With the high yield of hexagonal structure and electrically proven device quality of GaP NPs though this growth method, we believe this work represents a significant step in achieving GaP vertical NP optical devices, such as the promising green light micro LEDs.

Acknowledgment

The authors are indebted to IMEC for providing the SiO_2 patterned Si(111) substrates for this study.

References

[1] M. Cantoro *et al.*, "Controlled III/V nanowire growth by selective-area vapour phase epitaxy," *ECS Trans.*, vol. 19, no. 5, pp. 309–329, May 2009.

[2] D. V. Lang, H. G. Grimmeiss, E. Meijer, and M. Jaros, "Complex nature of gold-related deep levels in silicon," *Phys. Rev. B, Condens. Matter*, vol. 22, no. 8, pp. 3917–3934, Oct. 1980, doi: 10.1103/PhysRevB.22.3917.

[3] P. D. Dapkus *et al.*, "Selective area epitaxy by metalorganic chemical vapor deposition—A tool for photonic and novel nanostructure integration," *Prog. Quantum Electron.*, vol. 75, Jan. 2021, Art. no. 100304, doi: 10.1016/j.pquantelec.2020.100304.

[4] V. C. Elarde and J. J. Coleman, "Nanoscale selective area epitaxy for optoelectronic devices," *Prog. Quantum Electron.*, vol. 31, no. 6, pp. 225–257, Jan. 2007, doi: 10.1016/j.pquantelec.2007.08.001.

[5] X. Yuan *et al.*, "Selective area epitaxy of III–V nanostructure arrays and networks: Growth, applications, and future directions," *Appl. Phys. Rev.*, vol. 8, p. 021302, Apr. 2021, doi: 10.1063/5.0044706.

[6] K. P. Bassett, P. K. Mohseni, and X. Li, "Evolution of GaAs nanowire geometry in selective area epitaxy," *Appl. Phys. Lett.*, vol. 106, p. 133102, 2015.

[7] K. Tomioka, T. Tanaka, S. Hara, K. Hiruma, and T. Fukui, "III–V nanowires on Si substrate: Selective-area growth and device applications," *IEEE J. Sel. Topics Quantum Electron.*, vol. 17, no. 4, pp. 1112–1129, Jul. 2011, doi: 10.1109/JSTQE.2010.2068280.

[8] K. Tomioka, Y. Kobayashi, J. Motohisa, S. Hara, and T. Fukui, "Selective-area growth of vertically aligned GaAs and GaAs/AlGaAs core–shell nanowires on Si(111) substrate," *Nanotechnology*, vol. 20, no. 14, Apr. 2009, Art. no. 145302, doi: 10.1088/0957-4484/20/14/145302.

[9] S. Singh and P. Srivastava, "Optical properties of gallium phosphide (GaP) nanowires," *Appl. Nanosci.*, vol. 3, no. 2, pp. 89–94, Apr. 2013, doi: 10.1007/s13204-012-0096-6.

[10] J. Václavík and D. Vápenka, "Gallium phosphide as a material for visible and infrared optics," in *Proc. EPJ Web Conf.*, vol. 48, 2013, pp. 1–4, doi: 10.1051/epjconf/20134800028.

[11] G. Zhang, K. Tateno, T. Sogawa, and H. Nakano, "Growth and characterization of GaP nanowires on Si substrate," *J. Appl. Phys.*, vol. 103, no. 1, Jan. 2008, Art. no. 014301, doi: 10.1063/1.2828165.

[12] S. Assali *et al.*, "Direct band gap wurtzite gallium phosphide nanowires," *Nano Lett.*, vol. 13, no. 4, pp. 1559–1563, Apr. 2013, doi: 10.1021/nl304723c.

[13] F. Ishizaka, Y. Hiraya, K. Tomioka, and T. Fukui, "Growth of wurtzite GaP in InP/GaP core–shell nanowires by selective-area MOVPE," *J. Cryst. Growth*, vol. 411, pp. 71–75, Feb. 2015, doi: 10.1016/j.jcrysgro.2014.10.024.

[14] G. Priante, G. Patriarche, F. Oehler, F. Glas, and J.-C. Harmand, "Abrupt GaP/GaAs interfaces in self-catalyzed nanowires," *Nano Lett.*, vol. 15, no. 9, pp. 6036–6041, Sep. 2015, doi: 10.1021/acs.nanolett.5b02224.

[15] A. Standing *et al.*, "Efficient water reduction with gallium phosphide nanowires," *Nature Commun.*, vol. 6, no. 1, pp. 1–7, Nov. 2015, doi: 10.1038/ncomms8824.

[16] S. Assali *et al.*, "Optical study of the band structure of wurtzite GaP nanowires," *J. Appl. Phys.*, vol. 120, no. 4, Jul. 2016, Art. no. 044304, doi: 10.1063/1.4959147.

[17] U. Rizal, B. P. Swain, and B. S. Swain, "Gallium phosphide nanowires for optoelectronic devices," in *Proc. Int. Conf. Microelectron., Comput. Commun. (MicroCom)*, Jan. 2016, pp. 3–6.

[18] P. Kuyanov, J. Boulanger, and R. R. LaPierre, "Control of GaP nanowire morphology by group V flux in gas source molecular beam epitaxy," *J. Cryst. Growth*, vol. 462, pp. 29–34, Mar. 2017, doi: 10.1016/j.jcrysgro.2017.01.025.

[19] L. Gagliano, M. Albani, M. A. Verheijen, E. P. A. M. Bakkers, and L. Miglio, "Twofold origin of strain-induced bending in core–shell nanowires: The GaP/InGaP case," *Nanotechnology*, vol. 29, no. 31, Aug. 2018, Art. no. 315703, doi: 10.1088/1361-6528/aac417.

[20] N. N. Halder, A. Kelrich, S. Cohen, and D. Ritter, "Pure wurtzite GaP nanowires grown on zincblende GaP substrates by selective area vapor liquid solid epitaxy," *Nanotechnology*, vol. 28, no. 46, Nov. 2017, Art. no. 465603, doi: 10.1088/1361-6528/aa8b60.

[21] S. Ando, N. Kobayashi, and H. Ando, "Selective area metalorganic chemical vapor deposition growth for hexagonal-facet lasers," *J. Cryst. Growth*, vol. 145, nos. 1–4, pp. 302–307, 1994, doi: 10.1016/0022-0248(94)91067-7.

[22] K. Ikejiri *et al.*, "Growth characteristics of GaAs nanowires obtained by selective area metal–organic vapour-phase epitaxy," *Nanotechnology*, vol. 19, no. 26, 2008, Art. no. 265604, doi: 10.1088/0957-4484/19/26/265604.

[23] H. Yoshida *et al.*, "Analysis of twin defects in GaAs nanowires and tetrahedra and their correlation to GaAs(111)B surface reconstructions in selective-area metal organic vapour-phase epitaxy," *J. Cryst. Growth*, vol. 312, no. 1, pp. 52–57, Dec. 2009, doi: 10.1016/j.jcrysgro.2009.10.006.

[24] A. L. Greenaway *et al.*, "Selective area epitaxy of GaAs microstructures by close-spaced vapor transport for solar energy conversion applications," *ACS Energy Lett.*, vol. 1, no. 2, pp. 402–408, Aug. 2016, doi: 10.1021/acsenergylett.6b00217.

[25] C. Renard *et al.*, "Erratum: High current density GaAs/Si rectifying heterojunction by defect free epitaxial lateral overgrowth on tunnel oxide from nano-seed," *Sci. Rep.*, vol. 6, no. 1, p. 29875, Sep. 2016, doi: 10.1038/srep29875.

[26] D. Biegelsen, R. Bringans, J. Northrup, and L.-E. Swartz, "Reconstructions of GaAs($1^{-}1^{-}1^{-}$) surfaces observed by scanning tunneling microscopy," *Phys. Rev. Lett.*, vol. 65, no. 4, pp. 452–455, Jul. 1990.

[27] Q. Gao *et al.*, "Selective-area epitaxy of pure wurtzite InP nanowires: High quantum efficiency and room-temperature lasing," *Nano Lett.*, vol. 14, no. 9, pp. 5206–5211, Sep. 2014, doi: 10.1021/nl5021409.
[28] J. N. Shapiro, A. Lin, D. L. Huffaker, and C. Ratsch, "Potential energy surface of in and Ga adatoms above the (111)A and (110) surfaces of a GaAs nanopillar," *Phys. Rev. B, Condens. Matter*, vol. 84, no. 8, pp. 1–5, Aug. 2011, doi: 10.1103/PhysRevB.84.085322.
[29] K. Ikejiri, Y. Kitauchi, K. Tomioka, J. Motohisa, and T. Fukui, "Zinc blende and wurtzite crystal phase mixing and transition in indium phosphide nanowires," *Nano Lett.*, vol. 11, no. 10, pp. 4314–4318, Oct. 2011, doi: 10.1021/nl202365q.
[30] K. A. Dick, C. Thelander, L. Samuelson, and P. Caroff, "Crystal phase engineering in single InAs nanowires," *Nano Lett.*, vol. 10, no. 9, pp. 3494–3499, Sep. 2010, doi: 10.1021/nl101632a.
[31] A. De and C. E. Pryor, "Predicted band structures of III–V semiconductors in the wurtzite phase," *Phys. Rev. B, Condens. Matter*, vol. 81, no. 15, Apr. 2010, Art. no. 155210, doi: 10.1103/PhysRevB.81.155210.
[32] J. Johansson *et al.*, "Effects of supersaturation on the crystal structure of gold seeded III–V nanowires," *Cryst. Growth Des.*, vol. 9, no. 2, pp. 766–773, Feb. 2009, doi: 10.1021/cg800270q.
[33] V. G. Dubrovskii, N. V. Sibirev, J. C. Harmand, and F. Glas, "Growth kinetics and crystal structure of semiconductor nanowires," *Phys. Rev. B, Condens. Matter*, vol. 78, no. 23, pp. 1–10, Dec. 2008, doi: 10.1103/PhysRevB.78.235301.
[34] F. Glas, J.-C. Harmand, and G. Patriarche, "Why does wurtzite form in nanowires of III–V zinc blende semiconductors?" *Phys. Rev. Lett.*, vol. 99, no. 14, pp. 3–6, Oct. 2007, doi: 10.1103/PhysRevLett.99.146101.
[35] S. Lehmann, J. Wallentin, D. Jacobsson, K. Deppert, and K. A. Dick, "A general approach for sharp crystal phase switching in InAs, GaAs, InP, and GaP nanowires using only group v flow," *Nano Lett.*, vol. 13, no. 9, pp. 4099–4105, Sep. 2013, doi: 10.1021/nl401554w.
[36] P. Caroff, J. Bolinsson, and J. Johansson, "Crystal phases in III–V nanowires: From random toward engineered polytypism," *IEEE J. Sel. Topics Quantum Electron.*, vol. 17, no. 4, pp. 829–846, Jul. 2011, doi: 10.1109/JSTQE.2010.2070790.
[37] Y. Kitauchi *et al.*, "Structural transition in indium phosphide nanowires," *Nano Lett.*, vol. 10, no. 5, pp. 1699–1703, May 2010, doi: 10.1021/nl1000407.
[38] J. Johansson *et al.*, "Diameter dependence of the wurtzite–zinc blende transition in InAs nanowires," *J. Phys. Chem. C*, vol. 114, no. 9, pp. 3837–3842, Mar. 2010, doi: 10.1021/jp910821e.
[39] H. Shtrikman *et al.*, "Method for suppression of stacking faults in wurtzite III–V nanowires," *Nano Lett.*, vol. 9, no. 4, pp. 1506–1510, Apr. 2009, doi: 10.1021/nl803524s.
[40] K. Tomioka, J. Motohisa, S. Hara, K. Hiruma, and T. Fukui, "GaAs/AlGaAs core multishell nanowire-based light-emitting diodes on Si," *Nano Lett.*, vol. 10, no. 5, pp. 1639–1644, 2010, doi: 10.1021/nl9041774.

Wonsik Choi received the Ph.D. degree from the University of Illinois Urbana-Champaign in 2019. He joined Samsung Electronics after his Ph.D. graduation.

Hsien-Chih Huang (Graduate Student Member, IEEE) received the B.S. degree from National Taiwan University and the M.S. degree from the University of Illinois Urbana-Champaign, where he is currently pursuing the Ph.D. degree with a focus on wide bandgap material and nanofabrication.

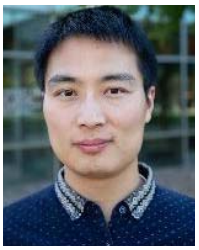

Shizhao Fan received the B.Eng. degree from the University of Science and Technology of China (USTC) in 2011 and the Ph.D. degree from McGill University, Montreal, QC, Canada, in 2016. He was with the Holonyak Micro and Nanotechnology Laboratory, University of Illinois at Urbana-Champaign (UIUC), as a Post-Doctoral Research Associate, from 2016 to 2020. He is currently a Research Scientist with the Suzhou Institute of Nano-Tech and Nano-Bionics (SINANO), CAS, and focus on the development of high-performance optoelectronic devices using the Vacuum Interconnected Nanotech Workstation (Nano-X).

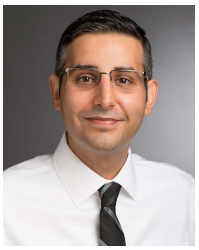

Parsian K. Mohseni received the B.Eng. and Ph.D. degrees in engineering physics from McMaster University. Following a post-doctoral research at the University of Illinois at Urbana-Champaign, he joined the faculty of the Rochester Institute of Technology (RIT) in 2015. He is currently an Associate Professor of electrical and microelectronic engineering and a Principal Investigator as a part of NanoPower Research Laboratories, RIT. His research on crystal growth of semiconductor nanomaterials, mixed-dimensional heterostructures, nanofabrication, and optoelectronic devices has resulted in over 50 publications to date.

Minjoo Larry Lee (Member, IEEE) received the B.Sc. degree (Hons.) in materials science and engineering from Brown University, Providence, RI, USA, in 1998, and the Ph.D. degree in electronic materials from the Massachusetts Institute of Technology (MIT), Cambridge, MA, USA, in 2003. From 2003 to 2006, he was a Post-Doctoral Researcher with the Microsystems Technology Laboratory, MIT. From 2006 to 2007, he was a Research Engineer with the Center for Thermoelectrics Research, RTI International, Durham, NC, USA. In 2008, he joined the EE Department, Yale University, New Haven, CT, USA. In 2016, he joined the ECE Department, University of Illinois at Urbana-Champaign, Urbana, IL, USA, where he is currently a Professor. He is the author or coauthor of more than 190 technical articles and conference proceedings, and holds nine patents. His previous research was on chemical vapor deposition growth techniques and high-mobility strained Si, SiGe, and Ge field-effect transistors. His current research interests include III–V molecular beam epitaxy (MBE) and III–V/Si integrated photonics. He is a member of the Materials Research Society (MRS). He has received recognitions, including the IBM Faculty Award, the North American Conference on MBE Young Investigator Award, the DARPA Young Faculty Award, the NSF CAREER Award, and the IEEE Electron Device Society George E. Smith Award. His advisees have won 12 best presentation prizes at international conferences.

Xiuling Li (Fellow, IEEE) received the B.S. degree from Peking University and the Ph.D. degree from the University of California at Los Angeles. Following post-doctoral positions at the California Institute of Technology and the University of Illinois, and industry experience at II-VI, Inc. (formerly Epi-Works, Inc.), she joined the faculty of the University of Illinois at Urbana-Champaign (UIUC) in 2007 and then relocated to The University of Texas (UT) at Austin in August 2021. She held the Donald Biggar Willett Professorship in engineering at the Department of Electrical and Computer Engineering (ECE) and the Interim Director of the Nick Holonyak Jr. Micro and Nanotechnology Laboratory, UIUC. She is currently the Temple Foundation Endowed Professor in ECE with UT. She has published more than 160 journal articles, holds more than 20 patents, and delivered more than 120 invited lectures worldwide. She is a fellow of the American Physics Society (APS), the Optical Society (OSA), the National Academy of Inventors (NAI), and the American Association for the Advancement of Science (AAAS). Her research has been honored with the NSF CAREER Award, the DARPA Young Faculty Award, and the ONR Young Investigator Award. She also serves as a Deputy Editor of *Applied Physics Letters*.